

Statistical evidence for O⁺ energization and outflow caused by wave-particle interaction in the high altitude cusp and mantle

M. Waara¹, R. Slapak¹, H. Nilsson¹, G. Stenberg¹, M. André², and I. A. Barghouthi³

¹Swedish Institute of Space Physics, Kiruna, Sweden

²Swedish Institute of Space Physics, Uppsala, Sweden

³Al Quds University, Jerusalem, Palestine

Received: 15 November 2010 – Revised: 16 March 2011 – Accepted: 28 April 2011 – Published: 30 May 2011

Abstract. We present a statistical study of the low (<1 Hz) frequency electric and magnetic field spectral densities observed by Cluster spacecraft in the high altitude cusp and mantle region. At the O⁺ gyrofrequency (0.02–0.5 Hz) for this region the electric field spectral density is on average 0.2–2.2 (mV m⁻¹)² Hz⁻¹, implying that resonant heating at the gyrofrequency can be intense enough to explain the observed O⁺ energies of 20–1400 eV. The relation between the electric and magnetic field spectral densities results in a large span of phase velocities, from a few hundred km s⁻¹ up to a few thousand km s⁻¹. In spite of the large span of phase velocity, the ratio between the calculated local Alfvén velocity and the estimated phase velocity is close to unity. We provide average values of a coefficient describing diffusion in ion velocity space at different altitudes, which can be used in studies of ion energization and outflow. The observed average waves can explain the average O⁺ energies measured in the high altitude (8–15 R_E) cusp/mantle region of the terrestrial magnetosphere according to our test particle calculations.

Keywords. Magnetospheric physics (Magnetosphere-ionosphere interactions)

1 Introduction

The ionospheric projection of the cusp is the region of most direct interaction between the solar wind and the Earth's atmosphere/ionosphere. In response to particle precipitation and imposed magnetospheric electric fields, ionospheric plasma may flow up from the ionosphere, but at velocities which are low enough that the ions are still gravitationally bound (Nilsson et al., 1996). The high electron temperatures caused by the soft (100 eV) cusp electron precipitation

are particularly effective in causing ion outflow (Strangeway et al., 2005; Nilsson et al., 1996; Blelly et al., 1996). For the ions to overcome gravity, further acceleration is needed. The energization needed for the particles to escape from the magnetosphere is even larger. Seki et al. (2002) discuss the further acceleration that is needed for the ions to escape into the magnetosheath rather than return to the Earth through the tail. The most important source for ionospheric ions likely to escape from the magnetosphere is the cusp region. Many papers have studied the heating and acceleration in the low and mid-altitude cusp, where Bouhram et al. (2004) represents an unusually complete coverage in altitude, up to 6.5 R_E. It is believed that transverse heating of ions is important for ion outflow and one of the probable explanations for transverse heating is wave-particle interaction. Many studies (see Chang et al., 1986; Barghouthi et al., 1998; Barghouthi, 2008; Bouhram et al., 2003b, 2004, and references therein) have investigated the effect of wave-particle interaction on the ion outflow. They considered the spectral density in the electric field to be responsible for the transverse ion heating. Wave-particle interaction is usually described by a quasi-linear velocity diffusion rate in ion velocity space, caused by waves around the ion gyrofrequency (Retterer et al., 1987; Chang et al., 1986).

As the transversely accelerated ions subsequently move outward, their transverse energy is gradually converted to parallel energy by the mirror force. Such transversely heated and subsequently outflowing ions are known as conics due to their shape in velocity space (see André and Yau, 1997; Yau and André, 1997; Moore et al., 1999). Earlier studies at lower altitudes (up to 5 R_E; Norqvist et al., 1996; André et al., 1998; Bouhram et al., 2003b) found that only a few percent of the observed spectral density around the oxygen ion gyrofrequency is needed to be in resonance with the ions to obtain the measured O⁺ energies. Bouhram et al. (2004) reported a saturation of transverse heating processes which was suggested to be caused by finite wavelength effects; when the



Correspondence to: M. Waara
(martin.waara@irf.se)

gyroradius becomes larger than the wavelength of the observed waves, the heating saturates. Nilsson et al. (2004, 2006) indicated that at some altitude above 5 R_E heating becomes more efficient again. In a recent case study, Waara et al. (2010) searched the high altitude cusp/mantle for the longest period with significantly enhanced perpendicular to parallel temperature ratio, an expected sign of local transverse heating. They used the data set of Nilsson et al. (2006), and found a case lasting about 20 min. It was found that 100% of the observed wave amplitude around the oxygen ion gyrofrequency could not explain the observed perpendicular ion temperatures using a simple ion cyclotron resonance model (Chang et al., 1986). Even using the extreme assumption that all the observed electric field wave amplitude is due to a coherent electric field at the oxygen gyrofrequency, the obtained heating was still not enough to explain the observations.

We follow up Waara et al. (2010) with a statistical study of the electric and magnetic field spectral densities in the frequency range below 1 Hz, in the general vicinity of the high altitude oxygen gyrofrequency. In this study we characterize the wave environment to see what is the typical wave activity in the region, and relate it to lower altitude observations. We put the previous study of Waara et al. (2010) and the case studies in a companion paper by Slapak et al. (2011) into this context to see how the spectral densities observed in the case studies compare to the average values for this region.

We investigate how the electric and magnetic spectral densities vary with altitude. Furthermore, we characterize the wave type and investigate how sporadic the waves are. Finally we calculate velocity diffusion coefficients, according to the theory by Retterer et al. (1987) based on the observed electric field spectral densities. These are compared with previously used velocity diffusion coefficients based on lower altitude measurements. The results from this study will provide useful input to any model of high altitude ion heating.

2 Instrumentation

We use data from the Cluster spacecraft. The four identical spacecraft are placed in a polar orbit $4 \times 19.6 R_E$ (Escoubet et al., 2001). Data from three different instruments, EFW (Electric Field and Wave experiment), FGM (Fluxgate Magnetometer), and CIS (Cluster Ion Spectrometry experiment) are used in this study. The electric field and wave experiment (EFW) is designed to measure the electric field. EFW records two orthogonal electric field components in the satellite spin plane. In our data set the sampling rate is 25 samples s^{-1} (Gustafsson et al., 2001). Engwall et al. (2009) showed that for a sunlit spacecraft in a cold tenuous plasma, the size of the enhanced wake arising behind the spacecraft due to cold drifting ions can be larger than the length of the EFW wire booms. The probes are then measuring the enhanced wake electric field instead of the electric field in the ambi-

ent plasma. This is not the case for our measurements in the cusp/mantle region where the temperature is high and there are strong fluxes of magnetosheath particles.

We also use data from the Cluster fluxgate magnetometer (FGM), which measure the magnetic field vector. In our data set the sampling rate is 22.4 samples s^{-1} (Balogh et al., 2001).

Furthermore, we use the data from Cluster Ion Spectrometry (CIS). The CIS instrument is described in detail in Rème et al. (2001). The CIS package consists of two different instruments, a time-of-flight ion Composition Distribution Function (CODIF), which can resolve the major magnetospheric ions; and the Hot Ion Analyzer (HIA), which has no mass resolution but higher angular and energy resolution. By using a time-of-flight technique CODIF can resolve H⁺, He⁺⁺, He⁺, and O⁺. The angular resolution is 22.5° and the energy coverage in the modes of interest to us is from 40 eV per charge up to 38 keV per charge.

2.1 Data sets

The data set consists of EFW and FGM wave data when outflowing O⁺ is seen in the energy spectrograms of the CIS/CODIF data. The data set covers a 3-year period (January to May in 2001 to 2003). This corresponds to orbits with apogee on the sunward side of the terminator plane. Only events with outflowing O⁺ lasting more than 1 h were selected, and such events were seen in about two-thirds of the orbits. The particle data set is described by Nilsson et al. (2006). The time series data of the electric and magnetic fields have been Fourier transformed to obtain frequency spectra. The record length in the Fourier transform is 1024 points. The spectral densities used in this study is an average of three partially overlapping records, shifted 512 with respect to each other. The DC-level (0 Hz) in the data is removed by subtracting the mean of each time window for both the EFW and the FGM data. Due to the large uncertainties in the spectral densities, for the lowest frequencies we tested to omit the two lowest frequencies (0.025 and 0.05 Hz) from the statistics but this did not significantly affect the results. Hence, we chose to include even these frequencies as the O⁺ gyrofrequencies at the highest altitudes in our data set fall in this range. The measured values at 0.25, 0.5, 0.75, and 1 Hz are affected by the satellite spin (4 s) and the values we use are interpolated values from the adjacent points.

The locations where the data were taken are shown in Fig. 1. A cylindrical coordinate system is used, with locations in X and $R = \sqrt{Y^2 + Z^2}$ (GSE) coordinates. A model magnetopause (the model of Shue et al. (1998), $B_z = -5$ nT, $n = 5$ cm⁻³ and $V_{sw} = 350$ km s^{-1}) is shown with a dotted gray line. Earth is indicated by the blue ball. In the high altitude cusp/mantle essentially all heavy ions are flowing outward. There are no trapped populations (Nilsson et al., 2006; Waara et al., 2010; Slapak et al., 2011).

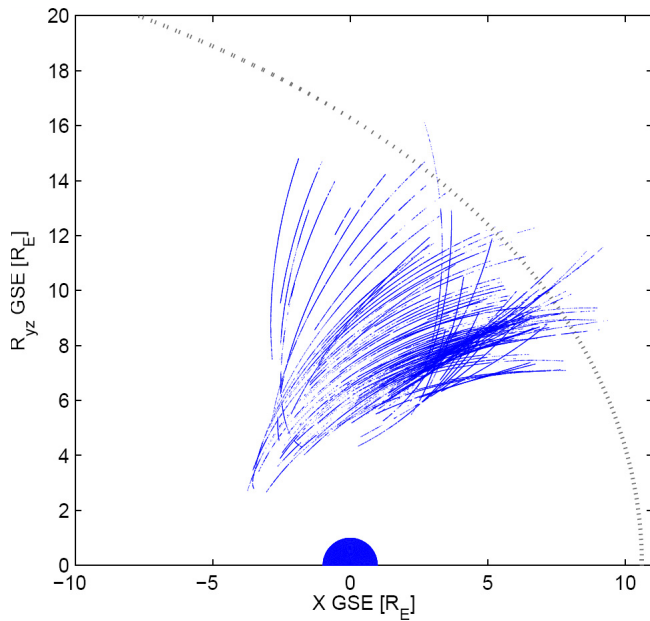


Fig. 1. The blue dots indicate where the data were taken in X and $R = \sqrt{Y^2 + Z^2}$ coordinates [R_E]. Earth is indicated by the blue ball.

3 Observations

The E and B spectral densities are connected through the characteristics of the waves giving rise to the electromagnetic wave activity. The ratio of the electric to magnetic wave intensity corresponds to the phase velocity of the electromagnetic wave, which can be used to identify the wave type.

The power spectral density for the electric field at the different altitudes in our data set is presented in the upper panel in Fig. 2. The different lines correspond to different altitudes. The frequency span is from 0.025 up to 1 Hz. The lower panel shows the average spectral density at the local oxygen gyrofrequency at each altitude. The average electric field spectral density increases with altitude. The highest average spectral density is about a factor of 3 to 4 higher than the lowest value. The spectral density versus frequency for the different altitudes is a power law and the slope of the different curves is approximately -1.5 .

Figure 3 shows the power spectral density of the magnetic field. There is about 3 orders of magnitude difference between the lowest and the highest values for the average magnetic field spectral density of the different altitude intervals. Just as for the electric field spectral density, the spectral density of the magnetic field versus frequency generally shows an approximate power law distribution. The slope of the spectral density versus frequency curves is similar at all altitudes, approximately -2 . The curves from the lowest altitudes are affected by the gradient of the geomagnetic field, and the values at the lowest frequencies are therefore overes-

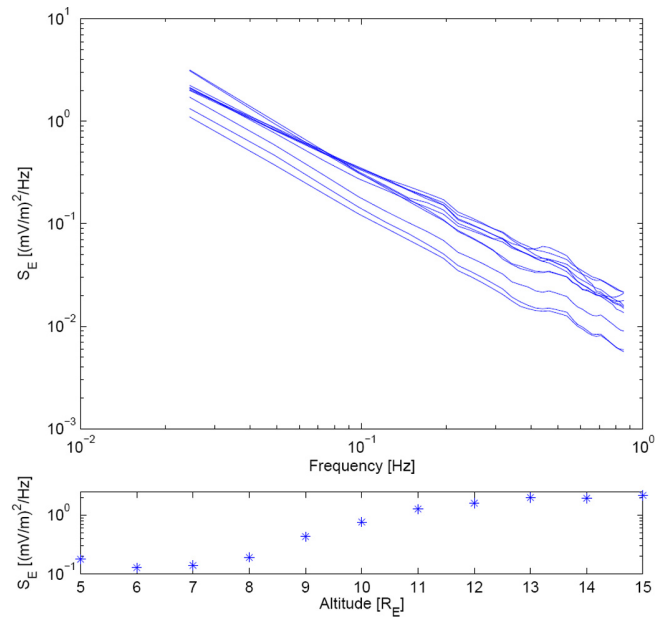


Fig. 2. Upper panel: The power spectral density for the electric field versus frequency observed at different geocentric distances (5–15 R_E). The slope of the curves is approximately -1.5 . Lower panel: The average spectral density at each altitude.

timated. The ambient magnetic field at the lowest altitudes is high enough that the wave magnetic field spectral density at the oxygen gyrofrequency is not affected by this overestimation. The average magnetic field spectral density at the local oxygen gyrofrequency shows a clear altitude dependence. The highest magnetic field spectral densities are observed at the highest altitudes, as can be seen in Fig. 3, lower panel.

The actual effect of the electric field wave intensity on ion distributions as function of altitude can be estimated by calculating a velocity diffusion rate to which the electric field of the waves gives rise. Figure 4 shows the electric field spectral density and the quasi-linear velocity diffusion rate perpendicular to the geomagnetic field given by Retterer et al. (1987):

$$D_{\perp} = \frac{\eta q^2}{4m^2} |E_x(\omega = \Omega)|^2 \quad (1)$$

where q is the charge, Ω is the ion gyrofrequency, ω is the wave frequency, $|E_x^2|$ is the electric field spectral density, and η is the proportion of the measured spectral density that corresponds to a left-hand polarized wave. The average electric field density for the different altitudes is in the span between 0.2 – 2.2 $(\text{mV m}^{-1})^2 \text{ Hz}^{-1}$ at the local oxygen gyrofrequency, (see Fig. 4). The local oxygen gyrofrequency is between 0.1 – 0.025 Hz at altitudes from 8 – $15 R_E$. We use a value of $\eta = 0.5$ in the calculations we show. The average diffusion coefficient shows an altitude dependence but a large span of values are observed at all altitudes. The standard deviation at each altitude is of the same order as the increase

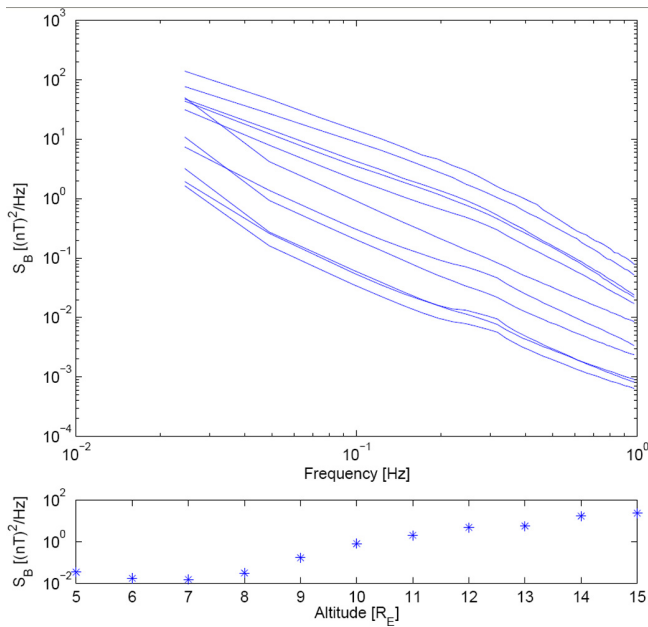


Fig. 3. Upper panel: the power spectral density for the magnetic field versus frequency observed at different geocentric distances (5–15 R_E). Lower panel: the average spectral density at each altitude.

of the diffusion coefficient from the lowest to the highest altitude, about an order of magnitude. As the distribution is approximately log-normal, we have calculated the average and standard deviations for the logarithmic values.

The diffusion coefficient and the electric field spectral density values for each altitude are presented in Table 1. The diffusion coefficient at the ion gyrofrequency is a factor of $\eta q^2/4m^2$ bigger than the spectral density (see Eq. 1).

3.1 Ion heating

We have used the model described by Chang et al. (1986) to calculate the heating of O⁺ from the average wave intensities. The theory used in this model is the same theory as Retterer et al. (1987), but Chang used a test particle simulation and Retterer used the velocity diffusion coefficient in a Monte Carlo simulation. This model assumes a broadband spectrum of waves around the gyrofrequency. The heating rate is given by:

$$\frac{dw}{dt} = S_L \frac{q^2}{2m} \quad (2)$$

where q and m are the charge and the mass of the ion and S_L is the power spectral density of the electric field at the O⁺ gyrofrequency due to left-hand polarized waves. The spectral densities used in the test particle calculation are the average spectral density presented in Fig. 4 and Table 1. Initial values and data points for comparison are taken from the statistical study of Nilsson et al. (2006), binned in altitude in the same way as the wave data. The particle data, with which

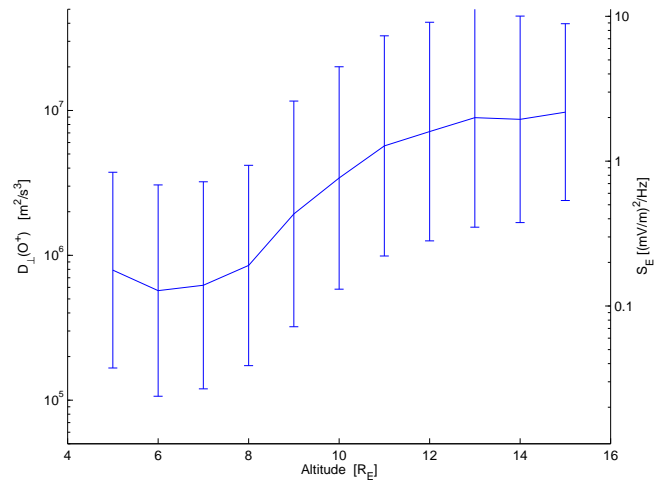


Fig. 4. Profile of the perpendicular diffusion coefficient for O⁺. The blue error bars show the standard deviation for the logarithmic value. The right axis is the values for diffusion coefficient and the left axis shows the corresponding electric field spectral density at the O⁺ gyrofrequency.

we will compare our test particle simulation results, are presented in Fig. 5 (O⁺ perpendicular temperature), Fig. 6 (O⁺ parallel velocity), and Fig. 7 (average background magnetic field). The starting point for the test particle calculation is 8 R_E and the measured values we have used as initial values are a perpendicular energy of 19 eV (Fig. 5), a parallel velocity of 43 km s⁻¹ (Fig. 6), and a magnetic field of 120 nT (Fig. 7). The end point for the calculation is 15 R_E . The magnetic field used in the calculation is the measured total average magnetic field at each altitude presented in Fig. 7. We have assumed that 50 % of the observed spectral density is effective in heating the ions. The test particle calculation presented in Table 1 shows that the particles are heated by the electric field spectral density from 19 eV up to 980 eV and that the parallel velocity is increased from 50 km s⁻¹ up to 93 km s⁻¹. The results from the calculation are just a bit smaller than the measured values at 15 R_E ($E_{\perp} = 1400$ eV and $V_{\parallel} = 113$ km s⁻¹), implying that resonant heating at the gyrofrequency can be intense enough to explain most of the observed O⁺ energies. The results of the test particle calculation are weakly dependent on the initial values since the resulting energy is much higher than the initial energy. The initial values for the test particle calculation and the results of the calculation are presented in Figs. 5, 6, and summarized in Table 1.

The fact that the calculated curve (black dots) in Fig. 6 is a little bit below the measured values can be due to centrifugal acceleration. The centrifugal acceleration in this region is described by Nilsson et al. (2008). The test particle calculation has also been made from 5–15 R_E , but then we must use the average spectral density plus the standard deviation to explain the observations. At the lowest altitudes

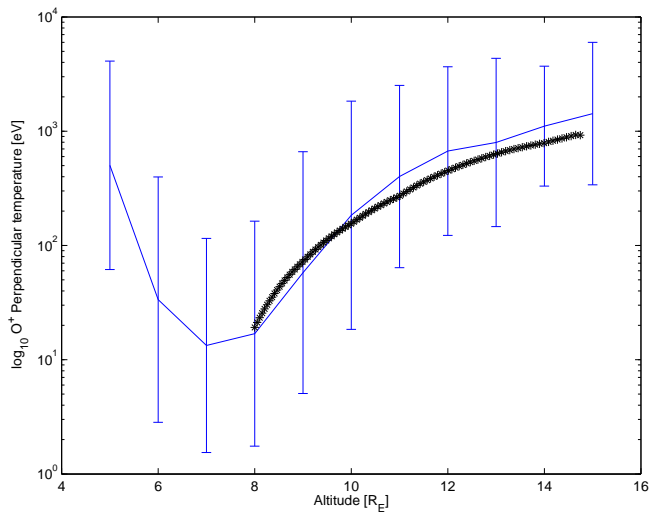


Fig. 5. Profile of the perpendicular temperature versus altitude. The blue error bars show the standard deviation for the logarithmic value. The black dots are the calculated perpendicular temperatures from the test particle calculation.

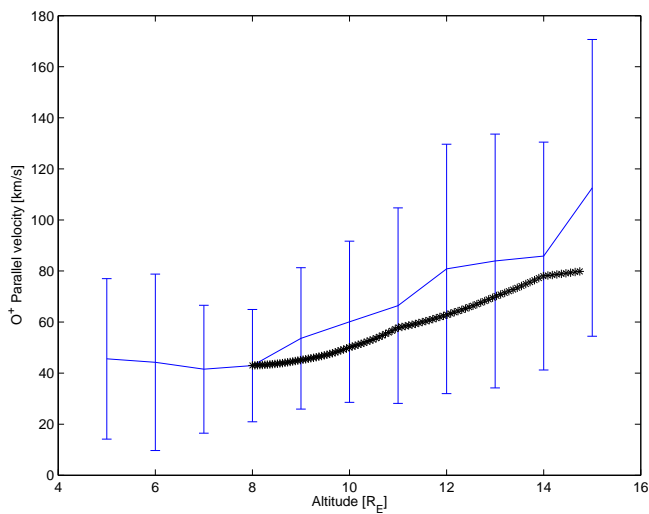


Fig. 6. Profile of the parallel velocity versus altitude. The blue error bars show the standard deviation for the linear values. The black dots are the calculated parallel velocities from the test particle calculation.

(5–8 R_E), our measurements are probably far into the polar cap, while higher altitude measurements correspond to both the cusp and the polar cap poleward of the cusp (see Fig. 1). Our estimates of the spectral density and temperature at the lowest altitudes are likely too small to be representative of the cusp at 5–8 R_E . A future study should also include the mid-altitude cusp.

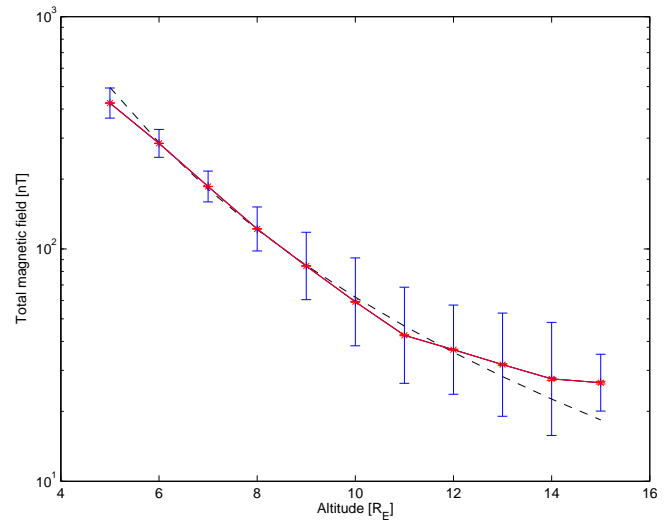


Fig. 7. Profile of the total magnetic field versus altitude. The blue error bars show the standard deviation for the logarithmic values. The black dashed line is the dipole model.

3.2 Relation between E and B

Figures 2 and 3 show the average electric and magnetic field spectral density as function of altitude. These two quantities are connected through the characteristics of the waves giving rise to the electromagnetic wave activity. The ratio of the electric to magnetic wave intensity corresponds to the phase velocity of the electromagnetic wave, which can then possibly be identified. It is a clear general impression from looking at the data that usually both the electric and magnetic field wave activity are enhanced simultaneously, but the relative amount of enhancement seems to vary. One way to investigate the wave type is by comparing the phase velocity (E/B) of the waves with the Alfvén velocity calculated from the background magnetic field and measured plasma parameters (see Fig. 8).

The background magnetic field used is the actual measured magnetic field, not a dipole model field. The field is presented in Fig. 7 and shows that for a magnetic field up to 12 R_E a dipole model is a good approximation. At higher altitudes the decrease of the measured background magnetic field with altitude is smaller than for a dipole field. Many of our measurements are from higher altitude than 12 R_E and we have chosen to use the average measured field values rather than the dipole model.

Figure 8 shows the observed E/B versus the Alfvén velocity (V_A) calculated from the observed geomagnetic field and density:

$$V_A = \frac{B}{(\mu_0 \rho)^{1/2}} \quad (3)$$

and Fig. 9 shows the average E/B -ratio (red) and Alfvén velocity (blue) for each altitude. The error bars show the

Table 1. Summary of the perpendicular diffusion coefficient for O⁺, the electric field spectral density at the local oxygen gyrofrequency, and summary of the test particle calculation.

Alt. [R_E]	S_E [(mV m ⁻¹) ² Hz ⁻¹]	$D_{\perp}(\text{O}^+)$ [m ² s ⁻³]	V_{\parallel} [km s ⁻¹]	E_{\perp} [eV]	V_{\parallel} [km s ⁻¹] calculated	E_{\perp} [eV] calculated
8	0.19	0.85×10^6	43	17	43	19
9	0.43	1.9×10^6	54	58	45	74
10	0.76	3.4×10^6	60	1.8×10^2	50	1.6×10^2
11	1.3	5.7×10^6	66	4.0×10^2	58	2.8×10^2
12	1.6	7.1×10^6	81	6.7×10^2	63	4.6×10^2
13	2.0	8.9×10^6	84	8.0×10^2	70	6.4×10^2
14	1.9	8.7×10^6	86	1.1×10^3	78	7.9×10^2
15	2.2	9.7×10^6	113	1.4×10^3	81	9.8×10^2

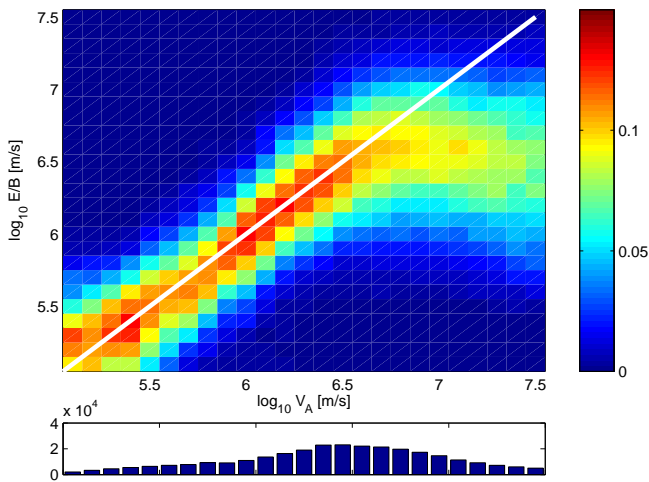


Fig. 8. Upper panel: the calculated Alfvén velocity [$\log \text{m s}^{-1}$] for each interval of E/B [$\log \text{m s}^{-1}$]. The color bar shows the occurrence frequency. Each column is normalized, that is, the sum of the values of all bins in a column is 1. The white line corresponds to the case when the phase velocity E/B and the calculated Alfvén velocity are equal. Lower panel: number of data points contributing to each column.

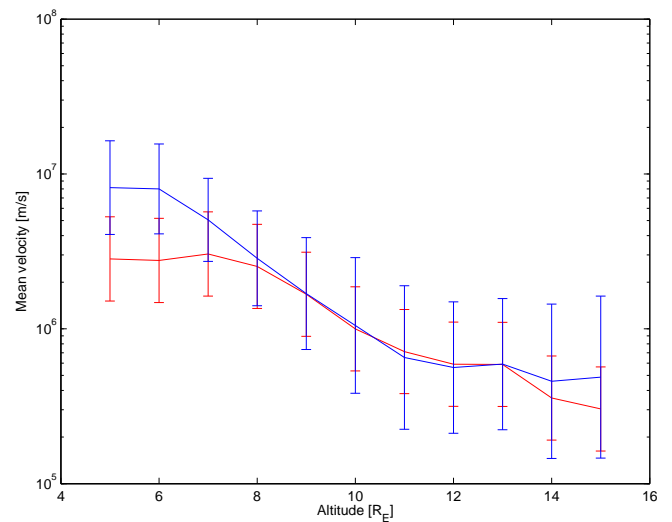


Fig. 9. The calculated mean Alfvén velocity [$\log \text{m s}^{-1}$] (blue) and mean E/B [$\log \text{m s}^{-1}$] (red) for each altitude. The blue and red error bars show the standard deviation for the logarithmic values.

standard deviation for the logarithmic values. The phase velocity varies from a few hundred km s⁻¹ up to a few thousand km s⁻¹, but the ratio between the calculated Alfvén velocity and the estimated phase velocity is close to unity. The observed waves in our data set above 8 R_E are consistent with Alfvén waves (Fig. 9). One may also note that our observations above 8 R_E are inconsistent with electric and magnetic field signatures due to static structures closing through the ionosphere. Such structures should give constant or an increasing E/B with altitude (Gurnett et al., 1984). This can be seen by considering how the electric and magnetic fields observed between two thin current sheets change with altitude. For the altitude range 5–8 R_E the calculated Alfvén velocity differs from E/B . A significant fraction of E/B

in this region can be due to static structures closing through the ionosphere and drifting past the spacecraft, or other wave modes. Investigating which other wave modes it may be is out of scope of this paper.

3.3 The time duration of the wave bursts

We have previously presented the average characteristics of the waves, including average velocity diffusion coefficients. We have also shown that the standard deviation of the wave activity is an order of magnitude, so that clearly the wave activity shows large variability. Visual inspection of the data shows that wave activity is typically enhanced in bursts. The length of bursts of enhanced wave activity, as measured in the spacecraft reference frame, is thus an important parameter describing the characteristics of the wave environment. In Fig. 10 we investigate the length of continuously observed

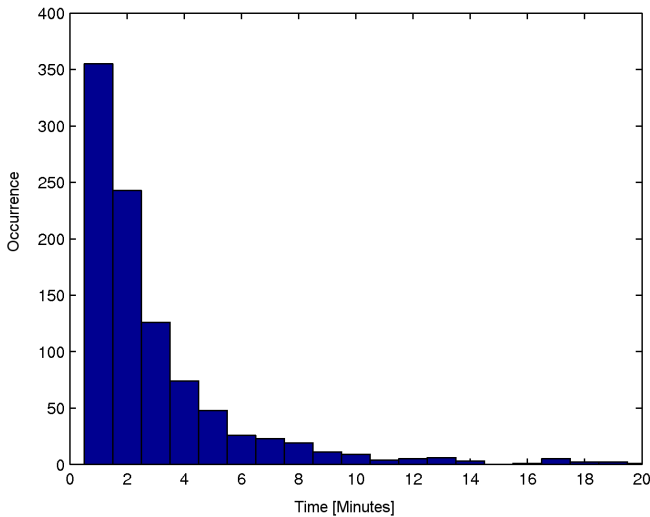


Fig. 10. Duration of continuously observed high electric field spectral density ($>3 \text{ (mV m}^{-1})^2 \text{ Hz}^{-1}$) at the O⁺ gyrofrequency.

high spectral densities. The observation time for the high spectral densities is important because if the waves are limited either in time or spatial extent, the actual heating may be difficult to observe. Figure 10 shows the duration for continuously measured high electric field spectral density ($>3 \text{ (mV m}^{-1})^2 \text{ Hz}^{-1}$) at the O⁺ gyrofrequency. There are just a few cases where high spectral density at the O⁺ gyrofrequency is observed longer than 10 min. Most of the events with high electric field spectral densities are shorter than 5 min, limited either in lifetime or spatial extent. In the companion paper (Slapak et al., 2011) it was shown that for the three cases investigated, the size of the region of enhanced wave activity was at least an order of magnitude larger than the O⁺ ion gyroradius.

4 Discussion

In a recent case study, Waara et al. (2010) searched for the longest period with significantly enhanced perpendicular to parallel ion temperature ratio in a data set based on high altitude cusp/mantle data from the Cluster spacecraft. The waves were left-hand polarized, at frequencies up to approximately the proton gyrofrequency, and the observed spectral density was $2 \text{ (mV m}^{-1})^2 \text{ Hz}^{-1}$ at the local O⁺ gyrofrequency. It was found that the observed wave amplitude around the oxygen gyrofrequency was not high enough to explain the observed perpendicular ion temperatures using a simple ion cyclotron resonance model. Waara et al. (2010) could not explain the observed perpendicular ion temperature, even using the extreme assumption that all the observed electric field wave amplitude is due to a coherent electric field at the gyrofrequency. Was the observed spectral density in the case study much lower than usual?

The electric field spectral density in the case study by Waara et al. (2010), $2 \text{ (mV m}^{-1})^2 \text{ Hz}^{-1}$, is a normal spectral density at high altitudes (10–15 R_E) as can be seen in Fig. 4. However, a perpendicular temperature of 8000 eV as observed in Waara et al. (2010) is much higher than the average value.

The relatively sporadic waves make it less likely to observe the actual heating. The heating from the waves can last for just a few minutes but the total energy gain for the particles remain, and the perpendicular temperature remains elevated for some time after the actual heating has stopped.

The model used in this paper assumes a broadband spectrum of waves around the gyrofrequency. The ion energization due to a broadband spectrum around the gyrofrequency involves a continuous transfer of energy from the fields to the ions. The effects of nonresonant fluctuations, where the fluctuations are well removed from the gyrofrequency, is very different. There are no continuous energy transfer from the fields to the ions. When the wave amplitude decreases, the ions decrease to their previous energy (Ball and Andre, 1991).

Due to the sporadic nature of the waves, and the fact that the ions can remain energized after the wave intensity has decreased, a good way of studying whether the waves can explain the highest observed temperatures is by finding cases with a high spectral density and looking to see if the simultaneously observed ions are heated. This was done in the companion paper of Slapak et al. (2011), and they found that they could explain some very high temperatures with the simultaneously observed waves.

The average spectral density versus frequency for the different altitudes (Fig. 2) showed that the spectral density increases for higher altitudes. It is a factor 3 to 4 between the highest and the lowest average spectral density; the electric field spectral density for the different altitudes generally have a power law distribution with a slope of -1.5 . The individual power spectral densities may differ from the power law but, as at lower altitudes, the average power density spectra has a clear power law distribution. Our frequency range is from 0.025 up to 1 Hz at altitudes from 5–15 R_E . The frequency span of the previous work of Barghouthi et al. (1998) was from 1 Hz up to 100 Hz at altitudes from 1.5 R_E to 4.5 R_E . Our data set is more or less a continuation in altitude of the data in Barghouthi et al. (1998). The average spectral density we obtain at 1 Hz is around 4–5 orders of magnitude smaller than what was reported from the auroral region in Barghouthi et al. (1998). In the polar wind, the value at 1 Hz presented there is 1–2 order of magnitude smaller than our estimate. Moreover, while we arrive a power law exponent of -1.5 , they get -3 . Hence, due to the different values at 1 Hz and the different power law exponents, it is not possible to easily extrapolate lower altitude measurements to higher altitudes.

Most previously published models of transverse ion heating at lower altitudes have assumed that the wave spectrum does not vary with altitude (André et al., 1990; Bouhram et al., 2003a; Crew et al., 1990), while Kasahara et al. (2001) showed with a statistical profile that the wave power remains constant versus altitude between 270 and 10 000 km in the dayside cusp/cleft. In our work the spectral density shows an altitude dependence but has a large standard deviation (i.e. case to case variation) at all altitudes. The standard deviation is of the same order as the increase or the spectral density from the lowest up to the highest altitude, about an order of magnitude. Therefore, to assume that the wave spectra are not altitude dependent is a good approximation, in particular for case studies of sudden heating events. However, for average properties, we suggest modelers to use our tabulated average velocity diffusion coefficients which take into account the altitude dependence of the wave spectra as well as the variation of the oxygen gyrofrequency.

The test particle calculation shows that by using the cyclotron model and the average spectral density measured at each altitude, we can explain the measured average perpendicular temperature and the parallel velocity. The standard deviation of the spectral density at each altitude spans over at least an order of magnitude, and using the average spectral density plus the standard deviation at each altitude in the test particle calculation gives much more ion energization than needed to explain the average perpendicular temperature. A recent case study (Slapak et al., 2011) showed that it is possible to explain even high perpendicular temperatures using the test-particle calculation, but not for all observed cases. Due to the weak magnetic field, the high energy of the particles, the consequent large oxygen ion gyroradius and the long gyroperiod, refinements of the cyclotron model are probably needed to fully explain the heating at the highest altitudes. A difference as compared to low altitude measurements is that we need to assume that almost all wave activity is due to waves which can interact with the ions, and of these we assume 50 % to be left-hand polarized.

There is a good correlation between the magnetic field spectral density and the electric field spectral density, as can be expected if the source of the wave activity is electromagnetic waves. The phase velocity, given by E/B , varies from a few hundred km s^{-1} up to a few thousand km s^{-1} in our data set. Even though the phase velocity changes by almost two orders of magnitude, there is still a good agreement when the calculated Alfvén velocity is compared with E/B of the waves. The ratio between the two velocities is close to unity for most cases. The observed waves are thus consistent with Alfvén waves.

5 Conclusions

We have characterized statistically the distribution of low frequency electric and magnetic field spectral densities in the

high altitude (5–15 R_E) cusp/mantle. It was found that the average electric field spectral density below 1 Hz is in the span between 0.2–2.2 $(\text{mV m}^{-1})^2 \text{Hz}^{-1}$. In only a few percent of the data set are the spectral densities above a few $(\text{mV m}^{-1})^2 \text{Hz}^{-1}$. High spectral densities were typically observed for periods of a few minutes. The relatively sporadic appearance of enhanced wave activity may make it difficult to observe the actual heating (as opposed to the results of previous heating).

The magnetic field spectral density varies much more with altitude than the electric field spectral density, but both parameters show an altitude dependence. The magnetic field density increases with 2.5 orders of magnitude over our altitude interval (5–15 R_E) while the difference between the highest and the lowest average electric field spectral density is a factor 3 to 4. The diffusion coefficient for O⁺ increases with altitude, about an order of magnitude between 5 and 15 R_E , but the standard deviation is large at all the altitudes, covering about an order of magnitude above and below the mean value.

The relation between the electric and magnetic field spectral densities results in a large span of phase velocities, from a few hundred km s^{-1} up to a few thousand km s^{-1} . In spite of the large span of phase velocity the ratio between the calculated local Alfvén velocity and the estimated phase velocity is close to unity. We also conclude that the altitude dependence of E/B , which decreases with altitude, is inconsistent with static structures of field-aligned currents closing through the ionosphere, at least above 5–8 R_E .

The electric field spectral density observed in the Waara et al. (2010) case study was around 2 $(\text{mV m}^{-1})^2 \text{Hz}^{-1}$. This is a relatively normal spectral density for this region, but their observed perpendicular temperature of 8000 eV is much higher than the average value. In the same study it was found that the observed spectral density around the oxygen gyrofrequency was far below what was needed to explain the observed perpendicular ion temperature using a simple ion resonance model. We have used the average spectral density in the same ion resonance model for calculation of the average perpendicular temperature and the average parallel velocity. The observed average waves can explain the observed average O⁺ energies measured in altitudes between 8–15 R_E of the cusp/mantle region, if we assume that 50 % of the observed wave activity at the local O⁺ gyrofrequency is due to left-hand polarized waves which can effectively heat the ions. The model probably needs refinements to fully fit the higher altitude conditions, in particular to explain the highest temperatures observed. However, the model can explain most of the observed heating when the average spectral density is used for each altitude. As at lower altitudes, the electric field spectral density as a function of frequency generally follows a power law distribution, but with lower intensity and a different power law index. Therefore the lower altitude measurements can not be extrapolated to high altitudes. We provide velocity diffusion coefficients based on high altitude

observations which can be used to model ion heating at high altitudes, rather than relying on extrapolation of low altitude data.

Acknowledgements. M. Waara, R. Slapak, and G. Stenberg were financed by the Swedish National Graduate School of Space Technology. H. Nilsson was supported by the Swedish Research Council. M. André was supported by the National Space Board of Sweden. Imad Barghouthi was supported by Swedish Research Links program. We also thank the EFW, FGM, and CIS instrument teams.

Topical Editor R. Nakamura thanks A. Yau and K. Lynch for their help in evaluating this paper.

References

- André, M. and Yau, A. W.: Theories and observations of ion energization and outflow in the high latitude magnetosphere, *Space Sci. Rev.*, 80, 27–48, 1997.
- André, M., Crew, G. B., Peterson, W. K., Persoon, A. M., and Pollock, C. J.: Ion heating by broadband low-frequency waves in the cusp/cleft, *J. Geophys. Res.*, 95, 20809–20823, doi:10.1029/JA095iA12p20809, 1990.
- André, M., Norqvist, P., Andersson, L., Eliasson, L., Eriksson, A. I., Blomberg, L., Erlandson, R. E., and Waldemark, J.: Ion energization mechanisms at 1700 km in the auroral region, *J. Geophys. Res.*, 103, 4199–4222, doi:10.1029/97JA00855, 1998.
- Ball, L. and André, M.: What parts of broadband spectra are responsible for ion conic production?, *Geophys. Res. Lett.*, 18, 1683–1686, doi:10.1029/91GL00169, 1991.
- Balogh, A., Carr, C. M., Acuña, M. H., Dunlop, M. W., Beek, T. J., Brown, P., Fornacon, K.-H., Georgescu, E., Glassmeier, K.-H., Harris, J., Musmann, G., Oddy, T., and Schwingenschuh, K.: The Cluster Magnetic Field Investigation: overview of in-flight performance and initial results, *Ann. Geophys.*, 19, 1207–1217, doi:10.5194/angeo-19-1207-2001, 2001.
- Barghouthi, I. A.: A Monte Carlo study for ion outflows at high altitude and high latitude: Barghouthi model, *Journal of Geophysical Research (Space Physics)*, 113, 8209, doi:10.1029/2008JA013274, 2008.
- Barghouthi, I. A., Barakat, A. R., and Persoon, A. M.: The Effects of Altitude-Dependent Wave Particle Interactions on the Polar Wind Plasma, *Astrophys. Space Sci.*, 259, 117–140, doi:10.1023/A:1001569207346, 1998.
- Blelly, P. L., Robineau, A., and Alcayde, D.: Numerical modelling of intermittent ion outflow events above EISCAT, *J. Atmos. Terr. Phys.*, 58, 273–285, 1996.
- Bouhram, M., Malingre, M., Jasperse, J. R., and Dubouloz, N.: Modeling transverse heating and outflow of ionospheric ions from the dayside cusp/cleft. 1 A parametric study, *Ann. Geophys.*, 21, 1753–1771, doi:10.5194/angeo-21-1753-2003, 2003a.
- Bouhram, M., Malingre, M., Jasperse, J. R., Dubouloz, N., and Sauvaud, J.-A.: Modeling transverse heating and outflow of ionospheric ions from the dayside cusp/cleft. 2 Applications, *Ann. Geophys.*, 21, 1773–1791, doi:10.5194/angeo-21-1773-2003, 2003b.
- Bouhram, M., Klecker, B., Miyake, W., Rème, H., Sauvaud, J.-A., Malingre, M., Kistler, L., and Blågä, A.: On the altitude dependence of transversely heated O⁺ distributions in the cusp/cleft, *Ann. Geophys.*, 22, 1787–1798, doi:10.5194/angeo-22-1787-2004, 2004.
- Chang, T., Crew, G. B., Hershkovitz, N., Jasperse, J. R., Retterer, J. M., and Winningham, J. D.: Transverse acceleration of oxygen ions by electromagnetic ion cyclotron resonance with broad band left-hand polarized waves, *Geophys. Res. Lett.*, 13, 636–639, doi:10.1029/GL013i007p00636, 1986.
- Crew, G. B., Chang, T., Retterer, J. M., Peterson, W. K., and Gurnett, D. A.: Ion cyclotron resonance heated conics – Theory and observations, *J. Geophys. Res.*, 95, 3959–3985, doi:10.1029/JA095iA04p03959, 1990.
- Engwall, E., Eriksson, A. I., Cully, C. M., André, M., Puhl-Quinn, P. A., Vaith, H., and Torbert, R.: Survey of cold ionospheric outflows in the magnetotail, *Ann. Geophys.*, 27, 3185–3201, doi:10.5194/angeo-27-3185-2009, 2009.
- Escoubet, C. P., Fehringer, M., and Goldstein, M.: Introduction: The Cluster mission, *Ann. Geophys.*, 19, 1197–1200, doi:10.5194/angeo-19-1197-2001, 2001.
- Gurnett, D. A., Huff, R. L., Menietti, J. D., Burch, J. L., Winningham, J. D., and Shawhan, S. D.: Correlated low-frequency electric and magnetic noise along the auroral field lines, *J. Geophys. Res.*, 89, 8971–8985, doi:10.1029/JA089iA10p08971, 1984.
- Gustafsson, G., André, M., Carozzi, T., Eriksson, A. I., Fälthammar, C.-G., Grard, R., Holmgren, G., Holtet, J. A., Ivchenko, N., Karlsson, T., Khotyaintsev, Y., Klimov, S., Laakso, H., Lindqvist, P.-A., Lybekk, B., Marklund, G., Mozer, F., Mursula, K., Pedersen, A., Popielawska, B., Savin, S., Stasiewicz, K., Tanskanen, P., Vaivads, A., and Wahlund, J.-E.: First results of electric field and density observations by Cluster EFW based on initial months of operation, *Ann. Geophys.*, 19, 1219–1240, doi:10.5194/angeo-19-1219-2001, 2001.
- Kasahara, Y., Hosoda, T., Mukai, T., Watanabe, S., Kimura, I., Kojima, H., and Niitsu, R.: ELF/VLF waves correlated with transversely accelerated ions in the auroral region observed by Akebono, *J. Geophys. Res.*, 106, 21123–21136, doi:10.1029/2000JA000318, 2001.
- Moore, T. E., Lundin, R., Alcayde, D., André, M., Ganguli, S. B., Temerin, M., and Yau, A.: Source processes in the high-altitude ionosphere, *Space Sci. Rev.*, 88, 7–84, 1999.
- Nilsson, H., Yamauchi, M., Eliasson, L., Norberg, O., and Clemmons, J.: The ionospheric signature of the cusp as seen by incoherent scatter radar, *J. Geophys. Res.*, 101, 10947–10963, 1996.
- Nilsson, H., Joko, S., Lundin, R., Rème, H., Sauvaud, J.-A., Dandouras, I., Balogh, A., Carr, C., Kistler, L. M., Klecker, B., Carlson, C. W., Bavassano-Cattaneo, M. B., and Korth, A.: The structure of high altitude O⁺ energization and outflow: a case study, *Ann. Geophys.*, 22, 2497–2506, doi:10.5194/angeo-22-2497-2004, 2004.
- Nilsson, H., Waara, M., Arvelius, S., Marghitu, O., Bouhram, M., Hobara, Y., Yamauchi, M., Lundin, R., Rème, H., Sauvaud, J.-A., Dandouras, I., Balogh, A., Kistler, L. M., Klecker, B., Carlson, C. W., Bavassano-Cattaneo, M. B., and Korth, A.: Characteristics of high altitude oxygen ion energization and outflow as observed by Cluster: a statistical study, *Ann. Geophys.*, 24, 1099–1112, doi:10.5194/angeo-24-1099-2006, 2006.
- Nilsson, H., Waara, M., Marghitu, O., Yamauchi, M., Lundin, R., Rème, H., Sauvaud, J.-A., Dandouras, I., Lucek, E., Kistler, L. M., Klecker, B., Carlson, C. W., Bavassano-Cattaneo, M. B., and Korth, A.: An assessment of the role of the centrifugal accel-

- ation mechanism in high altitude polar cap oxygen ion outflow, *Ann. Geophys.*, 26, 145–157, doi:10.5194/angeo-26-145-2008, 2008.
- Norqvist, P., André, M., Eliasson, L., Eriksson, A. I., Blomberg, L., Lühr, H., and Clemmons, J. H.: Ion cyclotron heating in the dayside magnetosphere, *J. Geophys. Res.*, 101, 13179–13194, doi:10.1029/95JA03596, 1996.
- Rème, H., Aoustin, C., Bosqued, J. M., Dandouras, I., Lavraud, B., Sauvaud, J. A., Barthe, A., Bouyssou, J., Camus, Th., Coeur-Joly, O., Cros, A., Cuvilo, J., Ducay, F., Garbarowitz, Y., Medale, J. L., Penou, E., Perrier, H., Romefort, D., Rouzaud, J., Vallat, C., Alcaydé, D., Jacquey, C., Mazelle, C., d’Uston, C., Möbius, E., Kistler, L. M., Crocker, K., Granoff, M., Mouikis, C., Popecki, M., Vosbury, M., Klecker, B., Hovestadt, D., Kucharek, H., Kuenneth, E., Paschmann, G., Scholer, M., Sckopke, N., Seidenschwang, E., Carlson, C. W., Curtis, D. W., Ingraham, C., Lin, R. P., McFadden, J. P., Parks, G. K., Phan, T., Formisano, V., Amata, E., Bavassano-Cattaneo, M. B., Baldetti, P., Bruno, R., Chionchio, G., Di Lellis, A., Marcucci, M. F., Pallochia, G., Korth, A., Daly, P. W., Graeve, B., Rosenbauer, H., Vasyliunas, V., McCarthy, M., Wilber, M., Eliasson, L., Lundin, R., Olsen, S., Shelley, E. G., Fuselier, S., Ghielmetti, A. G., Lennartsson, W., Escoubet, C. P., Balsiger, H., Friedel, R., Cao, J.-B., Kovrazhkin, R. A., Papamastorakis, I., Pellat, R., Scudder, J., and Sonnerup, B.: First multispacecraft ion measurements in and near the Earths magnetosphere with the identical Cluster ion spectrometry (CIS) experiment, *Ann. Geophys.*, 19, 1303–1354, doi:10.5194/angeo-19-1303-2001, 2001.
- Retterer, J. M., Chang, T., Crew, G. B., Jasperse, J. R., and Winningham, J. D.: Monte Carlo modeling of ionospheric oxygen acceleration by cyclotron resonance with broad-band electromagnetic turbulence, *Phys. Rev. Lett.*, 59, 148–151, doi:10.1103/PhysRevLett.59.148, 1987.
- Seki, K., Elphic, R. C., Thomsen, M. F., Bonnell, J., McFadden, J. P., Lund, E. J., Hirahara, M., Terasawa, T., and Mukai, T.: A new perspective on plasma supply mechanisms to the magnetotail from a statistical comparison of dayside mirroring O⁺ at low altitudes with lobe/mantle beams, *J. Geophys. Res. (Space Physics)*, 107, 1047, doi:10.1029/2001JA900122, 2002.
- Shue, J., Song, P., Russell, C. T., Steinberg, J. T., Chao, J. K., Zastenker, G., Vaisberg, O. L., Kokubun, S., Singer, H. J., Detman, T. R., and Kawano, H.: Magnetopause location under extreme solar wind conditions, *J. Geophys. Res.*, 103, 17691–17700, doi:10.1029/98JA01103, 1998.
- Slapak, R., Nilsson, H., Waara, M., André, M., Stenberg, G., and Barghouthi, I. A.: O⁺ heating associated with strong wave activity in the high altitude cusp and mantle, *Ann. Geophys.*, 29, 931–944, doi:10.5194/angeo-29-931-2011, 2011.
- Strangeway, R., Ergun, R. E., Su, Y. J., Carlson, C. W., and Elphic, R. C.: Factors controlling ionospheric outflows as observed at intermediate altitudes, *J. Geophys. Res.*, 110, A03221, doi:10.1029/2004JA010829, 2005.
- Waara, M., Nilsson, H., Stenberg, G., André, M., Gunell, H., and Rème, H.: Oxygen ion energization observed at high altitudes, *Ann. Geophys.*, 28, 907–916, doi:10.5194/angeo-28-907-2010, 2010.
- Yau, A. W. and André, M.: Sources of ion outflow in the high latitude ionosphere, *Space Sci. Rev.*, 80, 1–25, 1997.